W pair production at lepton colliders in the Feynman-diagram gauge

Hiroyuki Furusato[1,*], *Kentarou* Mawatari[1,2,3], *Yutaro* Suzuki[2], and *Ya-Juan* Zheng[3]

[1]Graduate School of Science and Engineering, Iwate University, Morioka, Iwate 020-8550, Japan
[2]Graduate School of Arts and Sciences, Iwate University, Morioka, Iwate 020-8550, Japan
[3]Faculty of Education, Iwate University, Morioka, Iwate 020-8550, Japan

Abstract. In ref. [1], we calculated helicity amplitudes for $e^-e^+ \to W^-W^+$ in the Feynman-diagram (FD) gauge analytically, and showed that the cross section can be understood by the individual γ, Z and ν amplitudes in the FD gauge. In this report, we discuss each contribution in the angular distributions in detail.

1 Introduction

W pair production at the electron-positron collider LEP played a crucial role in the construction of the $SU(2)\times U(1)$ gauge theory [2]. It will be also important for the precision test of the electroweak theory in future high-energy lepton colliders, such as the ILC [3–5], CEPC [6], and FCC-ee [7], to explore the physics beyond the standard model (SM).

In the $e^-e^+ \to W^-W^+$ process, there are contributions from the s-channel diagrams where γ and Z bosons propagate and the t-channel diagram where an electron-neutrino propagates; see Fig. 1. It is known that each of the three amplitudes has energy growth for longitudinally polarised W bosons. This seems to violate unitarity, but some cancellation among the amplitudes occurs, especially at high energies, resulting in a physical quantity. Since the magnitude of such cancellation is proportional to the energy, inaccuracy of numerical evaluations for cross sections as well as event generation becomes a problem for future high-energy collider experiments.

Recently, a new gauge fixing that does not cause gauge cancellation has been proposed, and it is called the "Feynman-diagram (FD)" gauge [8–10]. We note that most of the tree-level calculations and discussions have been conventionally done in the unitary (U) gauge. In ref. [1], we explicitly calculated helicity amplitudes for $e^-e^+ \to W^-W^+$ in the FD gauge and confirmed that no cancellation occurs in the high-energy region. Moreover, we showed that the Goldstone boson contribution is clearly visible even without taking the high-energy limit and the individual amplitudes follow the physical distribution, allowing for a physical interpretation of the amplitudes themselves. In this report, we discuss the individual contributions to the angular distributions in detail.

In the following, first, we indroduce the FD gauge in Sec. 2. Next, we show the helicity amplitudes for $e^-e^+ \to W^-W^+$ both in the FD and U gauges in Sec. 3. In Sec. 4 we present the numerical results to discuss the contributions from the individual Feynman amplitudes. Finally, a summary is given in Sec. 5.

*e-mail: s3124004@iwate-u.ac.jp; poster presenter at LCWS2024

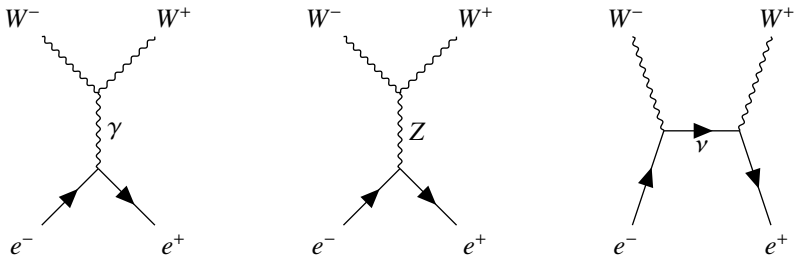

Figure 1. Feynman diagrams for $e^-e^+ \to W^-W^+$.

2 Feynman-diagram gauge

In this section, we briefly introduce ingredients necessary to calculate helicity amplitudes for the $e^-e^+ \to W^-W^+$ process in the FD gauge.

In the FD gauge, the propagator of the gauge bosons is obtained from the light-cone gauge [10], where the gauge vector is chosen along the opposite direction of the gauge-boson three momentum as

$$n^\mu = (\mathrm{sgn}(q^0), -\vec{q}/|\vec{q}|) \,. \tag{1}$$

Note that we take $n^\mu = (1, 0, 0, -1)$ when $|\vec{q}| = 0$ and $q^0 > 0$. The propagator of the photon is given by [8]

$$G_{\mu\nu}(q) = \frac{i}{q^2 + i\epsilon}\left(-g_{\mu\nu} + \frac{q_\mu n_\nu + n_\mu q_\nu}{n \cdot q}\right), \tag{2}$$

while that of the Z boson is combined with the associated Goldstone boson (π^0) and formed as a five-dimensional propagator [9]

$$G_{MN}(q) = \frac{i}{q^2 - m_Z^2 + i\epsilon}\begin{pmatrix} -g_{\mu\nu} + \dfrac{q_\mu n_\nu + n_\mu q_\nu}{n \cdot q} & i\dfrac{m_Z\, n_\mu}{n \cdot q} \\ -i\dfrac{m_Z\, n_\nu}{n \cdot q} & 1 \end{pmatrix}, \tag{3}$$

with $M, N = 0$ to 4, where 0 to 3 are the Lorentz indices μ, ν.

The polarization vector for the W bosons with the helicity $\lambda\,(= \pm 1, 0)$ in the FD gauge includes the associated Goldstone bosons ($\pi^\pm$), and is given as a five-component vector by [9],

$$\epsilon^M(p, \pm) = (\epsilon^\mu(p, \pm),\ 0) \,, \tag{4}$$

$$\epsilon^M(p, 0) = (\tilde{\epsilon}^\mu(p, 0),\ i) \,, \tag{5}$$

with the reduced polarization vector [8–10]

$$\tilde{\epsilon}^\mu(p, 0) = \epsilon^\mu(p, 0) - \frac{p^\mu}{m} \,, \tag{6}$$

where $\epsilon^\mu(p, \lambda)$ is the ordinary polarization vector.

3 Helicity amplitudes

In this section we present helicity amplitudes in the FD gauge for the process

$$e^-(k,\sigma) + e^+(\bar{k},\bar{\sigma}) \to W^-(p,\lambda) + W^+(\bar{p},\bar{\lambda}) \tag{7}$$

in the SM. The four-momenta (k, $\bar{k}$, p, $\bar{p}$) and the helicities (σ, $\bar{\sigma}$, λ, $\bar{\lambda}$) are defined in the e^-e^+ collision frame

$$\begin{aligned}
k^\mu &= \frac{\sqrt{s}}{2}(1,0,0,1)\,, \\
\bar{k}^\mu &= \frac{\sqrt{s}}{2}(1,0,0,-1)\,, \\
p^\mu &= \frac{\sqrt{s}}{2}(1,\beta\sin\theta,0,\beta\cos\theta)\,, \\
\bar{p}^\mu &= \frac{\sqrt{s}}{2}(1,-\beta\sin\theta,0,-\beta\cos\theta)\,,
\end{aligned} \tag{8}$$

with the center-of-mass energy $\sqrt{s}$ and the scattering angle θ for W^- with respect to the e^- momentum direction. The boost factors in this frame are

$$\beta = \sqrt{1-\frac{4m_W^2}{s}}\,, \quad \gamma = \frac{1}{\sqrt{1-\beta^2}} = \frac{\sqrt{s}}{2m_W}\,. \tag{9}$$

As shown in Fig. 1, there are three contributions to the process (7),

$$\mathcal{M} = \sum_i \mathcal{M}_i = \mathcal{M}_\gamma + \mathcal{M}_Z + \mathcal{M}_\nu\,. \tag{10}$$

We note that, although the Feynman diagrams look identical both in the FD and U gauges, the weak-boson lines in the FD gauge implicitly include the associated Goldstone bosons forming the 5×5 component propagator in eq. (3) and the five-component polarization vectors in eqs. (4) and (5).

Each helicity amplitude ($i = \gamma, Z, \nu$) is written as [11]

$$\mathcal{M}_{i\sigma}^{\lambda\bar{\lambda}} = \sqrt{2}\,e^2\,c_i\,\tilde{\mathcal{M}}_i^{\lambda\bar{\lambda}}(\theta)\,\varepsilon\,d^{J_0}_{\Delta\sigma,\Delta\lambda}(\theta)\,P_i(\theta)\,, \tag{11}$$

where the coupling factor c_i and the propagator factor $P_i(\theta)$ are given in Table 1, $\varepsilon = \Delta\sigma(-1)^{\bar{\lambda}}$ is a sign factor, $\Delta\sigma = (\sigma - \bar{\sigma})/2$, $\Delta\lambda = \lambda - \bar{\lambda}$, $J_0 = \max(|\Delta\sigma|, |\Delta\lambda|)$, and $d^{J_0}_{\Delta\sigma,\Delta\lambda}(\theta)$ is the d function. We note that, since we neglect the electron mass, $\bar{\sigma} = -\sigma$, i.e. $\Delta\sigma = +1$ or -1 and hence $J_0 = 1$ or 2. All the above factors in eq. (11) except the reduced helicity amplitudes $\tilde{\mathcal{M}}_i^{\lambda\bar{\lambda}}(\theta)$ are common both in the FD and U gauges. We present $\tilde{\mathcal{M}}_i^{\lambda\bar{\lambda}}(\theta)$ in the FD and U gauges in Table 2. In this report, we show amplitudes only for $\lambda = \bar{\lambda} = 0$; see ref. [1] for other helicity combinations. The sum of the three amplitudes (10) in the FD gauge agrees with that in the U gauge for each helicity combination because of the gauge invariance of the helicity amplitudes.

On the other hand, each amplitude (11) is rather different between the two gauges. The first term of each amplitude in the FD gauge is proportional to γ^{-2}, while that in the U gauge is proportional to γ^2. Therefore, in the high-energy regions ($\beta \to 1$, or $\gamma \to \infty$), the amplitudes behave rather differently in the two gauges.

In the U gauge, the Goldstone bosons do not present explicitly. However, in the FD gauge, the contribution of Goldstone bosons is manifest even without taking the high-energy limit.

Table 1. Coupling and propagator factors for each amplitude.

i	γ	Z	ν
c_i	1	$s_W^{-2}\left(-\frac{1}{2}\delta_{\sigma,-1}+s_W^2\right)$	$s_W^{-2}\delta_{\sigma,-1}$
$P_i(\theta)^{-1}$	1	$1-m_Z^2/s$	$1+\beta^2-2\beta\cos\theta$

Table 2. Reduced helicity amplitudes $\tilde{\mathcal{M}}_i{}^{\lambda\bar{\lambda}}(\theta)$ in eq. (11) for $\lambda=\bar{\lambda}=0$ in the FD and U gauges.

gauge	$\tilde{\mathcal{M}}_\gamma{}^{00}(\theta)$	$\tilde{\mathcal{M}}_Z{}^{00}(\theta)$	$\tilde{\mathcal{M}}_\nu{}^{00}(\theta)$
FD	$\frac{1}{\gamma^2}\frac{3+\beta}{(1+\beta)^2}+1$	$-\frac{1}{\gamma^2}\frac{3+\beta}{(1+\beta)^2}-\frac{s_W^2}{c_W^2}\left(\frac{\beta}{2s_W^2}-1\right)$	$-\frac{1}{\gamma^2}\frac{2}{(1+\beta)^2}(1+\cos\theta)$
U	$-2\gamma^2\beta+\beta$	$2\gamma^2\beta-\beta$	$2\gamma^2(\beta-\cos\theta)-\beta$

Table 3. Vertices for π^-- W^+- γ/Z, W^-- π^+- γ/Z and π^-- π^+- γ/Z, where the four-momenta is given in eq. (7).

$V_{VVV}^{M_1M_2M_3}$		W^-W^+A	W^-W^+Z
$V^{4\mu_2\mu_3}$	$ag^{\mu_2\mu_3}$	$a=\frac{g^2s_Wv}{2}$	$a=-\frac{g^2s_W^2v}{2c_W}$
$V^{\mu_14\mu_3}$	$ag^{\mu_1\mu_3}$	$a=-\frac{g^2s_Wv}{2}$	$a=\frac{g^2s_W^2v}{2c_W}$
$V^{44\mu_3}$	$ib(p-\bar{p})^{\mu_3}$	$b=gs_W$	$b=\frac{gc_{2W}}{2c_W}$

The second term of the s-channel γ/Z amplitudes in Table 2 is exactly a contribution of the Goldstone bosons. We show the vertices of π^-- W^+- γ/Z, W^-- π^+- γ/Z and π^-- π^+- γ/Z in Table 3, and the index "4" denotes the contribution of Goldstone bosons. As energy increases, the first term of the γ/Z amplitudes rapidly falls as γ^{-2} and the second term becomes dominant. This is consistent with the Goldstone boson equivalence theorem. We note that the Z-associated π^0 contribution is absent since we neglect the electron mass. Similarly, the $\pi^\pm$ do not couple to the massless fermion line in the ν-exchange diagram.

4 Cross sections

In this section we present the total and differential cross sections for $e^-e^+\to W^-W^+$ for $(\lambda,\bar{\lambda})=(0,0)$. The physical cross section is the absolute value square of the sum of the three amplitudes, and it is gauge invariant. We also show contributions from the absolute value square of the individual Feynman amplitude to compare the difference between the FD and U gauges.

Figure 2 shows the total cross section of $e^-e^+\to W^-W^+$ for $(\lambda,\bar{\lambda})=(0,0)$ as a function of the collision energy from 100 GeV to 400 GeV (left) and from 200 GeV up to 10 TeV (right), where the 100% polarized beams are assumed as the left-handed electron and the right-handed positron. The black solid line denotes the physical total cross section. Red, blue, and green dashed lines show contributions from the square of each γ, Z, and ν amplitude, respectively, in the FD gauge. Similarly, the dotted lines denote the U-gauge amplitudes.

The total cross section is identical between the two gauges, showing gauge invariance of the sum of all the amplitudes, and falls as $1/s$ for $s\gg m_Z^2$.

On the other hand, all three individual amplitude squares in the U gauge grow with energy, dictated by the γ^2 factor of the amplitudes in Table 2.

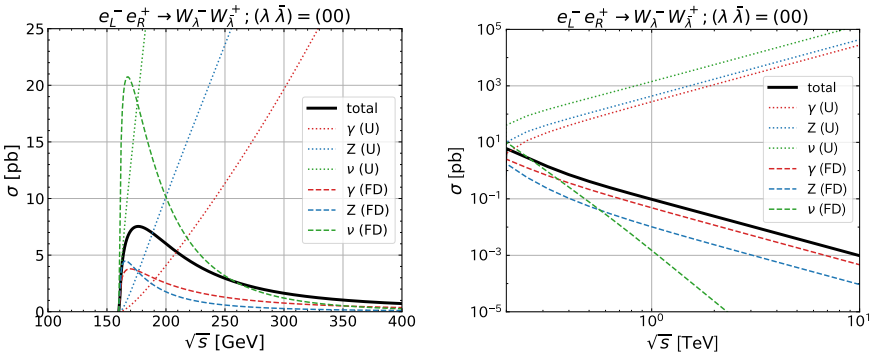

Figure 2. Total cross sections of $e^-e^+ \to W^-W^+$ for $(\lambda, \bar\lambda) = (0, 0)$ as a function of the collision energy with the left-handed electron. The range of the collision energies is from 100 GeV to 400 GeV (left) and from 200 GeV up to 10 TeV [1] (right). The solid line denotes the total cross section, dashed (dotted) lines show contributions from the absolute value square of the individual amplitude in the FD (U) gauge.

There is a slight constant difference between the photon (red dotted) and Z (blue dotted) contributions when $s \gg m_Z^2$. Since the reduced γ and Z amplitudes in Table 2 are identical except for the relative sign, these can be explained by the gauge couplings of electrons and the propagator factors in Table 1. This indicates that artificial gauge cancellation among the individual amplitudes to get the physical value in the U gauge. This is exactly a problem of numerical calculation which we have encountered at future high-energy colliders [12].

In the FD gauge, in contrast, the photon and Z contributions fall as $1/s$ in high energies, the same as the total cross section, while the ν contribution falls as $1/s^3$. There is absolutely no artificial cancellation among the relevant amplitudes, except the threshold region. We clearly see that the Goldstone-boson contributions and they become dominant when $\gamma^{-2} = 4m_W^2/s \ll 1$. Similar to the U gauge, the pure gauge-boson terms (the first terms), are identical except for the relative sign. On the other hand, for the Goldstone-boson terms, the Z amplitudes are suppressed by s_W^2/c_W^2 as compared to the photon ones, leading to a visible difference between the photon (red dashed) and the Z (blue dashed) contributions. The interference between amplitudes can be explained by the relative sign of the Goldstone-boson contributions and the coupling factors in Table 1 between photon and Z.

We now move to the differential cross section for $(\lambda, \bar\lambda) = (0, 0)$ at certain fixed energies. Figure 3 shows the distribution of the scattering angle of W^- with respect to the e^- momentum direction, defined in eq. (8), for $e^-e^+ \to W^-W^+$ at $\sqrt{s} = 250$ GeV (left) and $\sqrt{s} = 1$ TeV (right). The line types and colors are same as in Fig. 2.

As expected, the total (physical) distribution, denoted by the black solid line, is identical between the FD and U gauges. Since the d function in eq. (11) is common for all the amplitudes and $d^1_{-1,0}(\theta) = \sin\theta/\sqrt{2}$, the amplitudes vanish at $\cos\theta = \pm 1$. However, the physical distribution is rather distorted from the naive expectation of $\sin^2\theta$; the enhancement in the forward region ($\cos\theta \sim 1$) and a sharp dip structure are observed at both energies.

The angular distribution for the s-channel γ and Z amplitudes (red and blue) is simply determined by the d function. Thus the only difference between the FD and U gauges is the magnitude. The difference between the two gauges becomes larger at higher energies because of the difference of the γ dependence of the amplitudes as shown in Table 2.

For the t-channel ν amplitudes, the angular distributions are nontrivial. Because they are determined by some factors; i.e. the d function, the propagator factor $P_\nu(\theta)$ and the reduced amplitude $\tilde{\mathcal{M}}_\nu{}^{\lambda\bar\lambda}(\theta)$. However, the distribution in the U gauge (green dotted) is almost

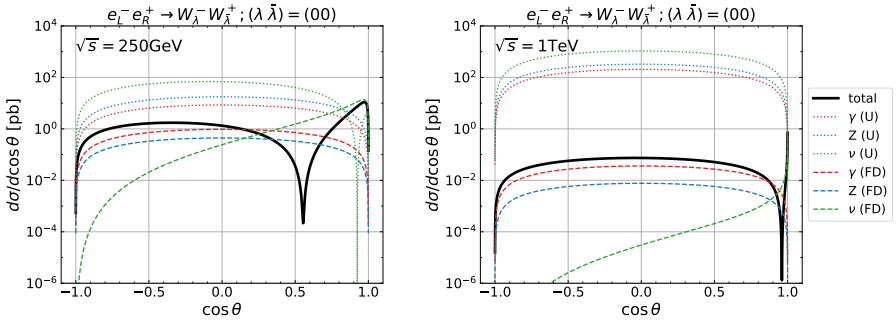

Figure 3. Distribution of the scattering angle of $e^-e^+ \to W^-W^+$ for $(\lambda, \bar\lambda) = (0, 0)$ with the left-handed electron at $\sqrt{s} = 250$ GeV (left) and at $\sqrt{s} = 1$ TeV (right). The solid line denotes the total distribution, while dashed (dotted) lines show contributions from the absolute value square of the γ amplitude (red), Z amplitude (blue) and ν amplitude (green) in the FD (U) gauge.

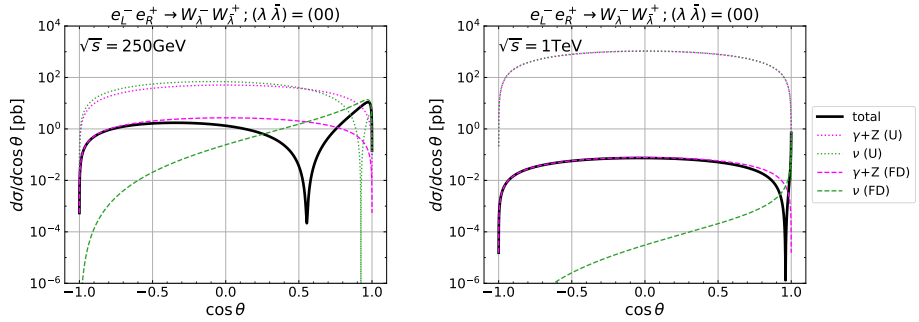

Figure 4. Same as Fig. 3, but the magenta lines show contributions from the absolute value square of the s-channel $\gamma + Z$ amplitude [1].

dominated by the d function. In contrast, for the ν contribution in the FD gauge (green dashed), we clearly see the enhancement in the forward region ($\cos\theta \sim 1$) and the suppression in the backward region ($\cos\theta \sim -1$) as naively expected from the t-channel propagator factor.

Instead of showing the three individual contributions $|\mathcal{M}_i|^2$ as in Fig. 3, we categorize the contributions based on th channels: the s-channel $\gamma + Z$ amplitude as $|\mathcal{M}_\gamma + \mathcal{M}_Z|^2$ (magenta) and t-channel ν (green), in Fig. 4. We can see clealy that the location of the physical dip position is at the crossing point of the dashed magenta line and green line. This explains the physical interference between the two channels in the FD gauge that creates the dip structure.

5 Summary

We presented the helicity amplitudes of the $e^-e^+ \to W^-W^+$ process in the FD gauge analytically for longitudinally polarized W bosons [1], and discussed the individual contributions to the angular distributions in detail.

Table 2 shows the FD-gauge amplitudes, and one can explicitly see that the well-known energy growth of the individual photon, Z, and ν exchange amplitudes for longitudinally polarized W bosons in the U gauge is completely absent in the FD gauge. One can also see that the Goldstone-boson contributions are manifest in the FD gauge even without taking the high-energy limit. The energy dependence of the individual amplitudes is explicitly shown in Fig. 2.

We also showed the differential cross sections in Figs. 3 and 4. The individual FD-gauge amplitudes give a more clear physics interpretations than the U gauge. In the forward region, the t-channel ν amplitude dominates. On the other hand, in the central and backward region, the s-channel $\gamma + Z$ amplitude dominates. The dip structure can be explained as being created by the physical interference of s-channel amplitude and t-channel amplitude of the same magnitude.

We hope that our results help to deepen our understanding at future high-energy lepton-collider experiments.

Acknowledgements

This work is supported in part by JSPS KAKENHI Grants No. 21H01077, No. 21K03583, No. 23K03403, No. 23K20840, and No. 24K07032.

References

[1] H. Furusato, K. Mawatari, Y. Suzuki, Y.J. Zheng, W-boson pair production at lepton colliders in the Feynman-diagram gauge, Phys. Rev. D **110**, 053005 (2024), 2406.08869. 10.1103/PhysRevD.110.053005

[2] S. Schael et al. (ALEPH, DELPHI, L3, OPAL, LEP Electroweak), Electroweak Measurements in Electron-Positron Collisions at W-Boson-Pair Energies at LEP, Phys. Rept. **532**, 119 (2013), 1302.3415. 10.1016/j.physrep.2013.07.004

[3] The International Linear Collider Technical Design Report - Volume 2: Physics (2013), 1306.6352.

[4] K. Fujii et al., Physics Case for the 250 GeV Stage of the International Linear Collider (2017), 1710.07621.

[5] A. Aryshev et al. (ILC International Development Team), The International Linear Collider: Report to Snowmass 2021 (2022), 2203.07622.

[6] M. Dong et al. (CEPC Study Group), CEPC Conceptual Design Report: Volume 2 - Physics & Detector (2018), 1811.10545.

[7] A. Abada et al. (FCC), FCC-ee: The Lepton Collider: Future Circular Collider Conceptual Design Report Volume 2, Eur. Phys. J. ST **228**, 261 (2019). 10.1140/epjst/e2019-900045-4

[8] K. Hagiwara, J. Kanzaki, K. Mawatari, QED and QCD helicity amplitudes in parton-shower gauge, Eur. Phys. J. C **80**, 584 (2020), 2003.03003. 10.1140/epjc/s10052-020-8154-9

[9] J. Chen, K. Hagiwara, J. Kanzaki, K. Mawatari, Helicity amplitudes without gauge cancellation for electroweak processes, Eur. Phys. J. C **83**, 922 (2023), [Erratum: Eur.Phys.J.C 84, 97 (2024)], 2203.10440. 10.1140/epjc/s10052-023-12093-7

[10] J. Chen, K. Hagiwara, J. Kanzaki, K. Mawatari, Y.J. Zheng, Helicity amplitudes in light-cone and Feynman-diagram gauges, Eur. Phys. J. Plus **139**, 332 (2024), 2211.14562. 10.1140/epjp/s13360-024-05067-5

[11] K. Hagiwara, R.D. Peccei, D. Zeppenfeld, K. Hikasa, Probing the Weak Boson Sector in $e^+e^- \to W^+W^-$, Nucl. Phys. B **282**, 253 (1987). 10.1016/0550-3213(87)90685-7

[12] K. Hagiwara, J. Kanzaki, O. Mattelaer, K. Mawatari, Y.J. Zheng, Automatic generation of helicity amplitudes in the Feynman-diagram gauge, Phys. Rev. D **110**, 056024 (2024), 2405.01256. 10.1103/PhysRevD.110.056024